Phase-field modeling of Mn-Ni-Si rich precipitate in neutron-irradiated RPV steel

Kunok Chang, Junhyun Kwon, Gyeong-Geun Lee

Korea Atomic Energy Research Institute, Daejeon, Korea, 34057
Corresponding author: kunokchang@kaeri.re.kr

1. Introduction

Irradiation-enhanced precipitation hardening is known as one of the main sources of the late-stage embrittlement of reactor pressure vessel (RPV) steel [1, 2, 3, 4, 5]. Even in low-Cu steel, Mn-Ni-Si (MNS) precipitates can be present in the stable form [3, 4, 5], and the MNS phases in RPV steel have been investigated using experimental [4, 5] and computational[3] methods. Xiong et al. assessed the thermodynamic database for the Fe-Mn-Ni-Si quaternary system, i.e., the UW1 database, and the results were compared with the output of the commercialized database TCAL2 [3]. In this study, we adopt the phase-field method to describe both thermodynamic and kinetic features of the Fe-Mn-Ni-Si quaternary system. Cu-containing precipitates of the low alloy Fe have already been investigated using the phase-field method [6, 7, 8]. Koyama et al. assessed the thermodynamic database for the Fe-Cu-Mn-Ni quaternary system [6, 7], and the phase-field method was used to investigate the kinetic and elastic aspects of the Fe-Cu-Mn-Ni system. We extended the binary KKS model [9] to the quaternary system to perform the simulation for the Fe-Mn-Ni-Si system. We considered four phases (one matrix and three precipitate phases) in our simulation. We proposed the framework that enables us to predict the stability of the precipitates in RPV steel by considering both thermodynamics and kinetics. The UW1 thermodynamic database [3] was used to perform the simulations of the precipitate behavior in the bcc Fe matrix of the quaternary system. We compared the stability of various types of precipitates in a low-alloy steel. Further, our predicted precipitate stability was compared with the prediction results of thermodynamic modeling [3] and experimental observations [4, 5].

2. UW1 CALPHAD database

We adopted the UW1 CALPHAD database to simulate the microstructural evolution of the Fe-Mn-Ni-Si system [3]. One bcc phase for the matrix and 12 MNS precipitate phases are considered. In our study, we selected one bcc phase and three MNS precipitate phases for simplicity. The thermodynamic parameters we used were taken from the supplementary material of ref. [3] as follows:

For bcc (Fe,Mn,Ni,Si) phase,

$$
\begin{aligned}
{}^0L^{bcc}_{Fe,Mn} &= -2759 + 1.23T \\
{}^0L^{bcc}_{Fe,Ni} &= -956.63 - 1.28726T \\
{}^1L^{bcc}_{Fe,Ni} &= 1789.03 - 1.92912T \\
{}^0L^{bcc}_{Fe,Si} &= -153138.56 + 46.48T \\
{}^1L^{bcc}_{Fe,Si} &= -92352 \\
{}^2L^{bcc}_{Fe,Si} &= 62240 \\
{}^0L^{bcc}_{Mn,Ni} &= -3508.43 - 23.7885T \\
{}^0L^{bcc}_{Mn,Si} &= -89620.7 + 2.9410T \\
{}^1L^{bcc}_{Mn,Si} &= -7500.0 \\
{}^0Tc^{bcc}_{Fe,Mn} &= 123 \\
{}^0Tc^{bcc}_{Fe,Si} &= 504
\end{aligned}
$$

For $T3 : Mn_{6/29}Ni_{16/20}Si_{7/20}$ phase,

$$
\begin{aligned}
{}^0G^{T3}_{Mn,Ni,Si} = -48186.497 &+ 6/29\,{}^0G^{cbcc}_{Mn} \\
&+ 16/29\,{}^0G^{fcc}_{Ni} + 7/29\,{}^0G^{diamond}_{Si}
\end{aligned}
$$

For $T6 : Mn_{1/3}(Ni, Si)_{2/3}$ phase,

$$
\begin{aligned}
{}^0G^{T6}_{Mn,Ni} &= 10086.99 + 1/3\,{}^0G^{cbcc}_{Mn} + 2/3\,{}^0G^{fcc}_{Ni} \\
{}^0G^{T6}_{Mn,Si} &= 1666.67 + 1/3\,{}^0G^{cbcc}_{Mn} + 2/3\,{}^0G^{fcc}_{Si} \\
{}^0L^{bcc}_{Mn:Ni,Si} &= -159474.81, {}^1L^{bcc}_{Mn:Ni,Si} = -172110.47
\end{aligned}
$$

For $T7 : Mn_{1/2}Ni_{1/3}Si_{1/6}$ phase,

$$
\begin{aligned}
{}^0G^{T7}_{Mn,Ni,Si} = -32434.25 - 5T &+ 1/2\,{}^0G^{cbcc}_{Mn} \\
&+ 1/3\,{}^0G^{fcc}_{Ni} + 1/6\,{}^0G^{diamond}_{Si}
\end{aligned}
$$

3. Phase-field model

We utilized the phase-field model to simulate the microstructural evolution of the Fe-Mn-Ni-Si system. We solved the Cahn-Hilliard [10] and Allen-Cahn (Ginzburg-Landau) equations [11] to simulate the microstructural evolution.

We will denote the composition (i = 1, 2, 3, 4 for Fe, Mn, Ni, Si, respectively) in the phase θ using $c_i^\theta(\mathbf{r}, t)$ at position $\mathbf{r}$ and time t. θ indicates the T3, T6, and T7 phases. We introduce four non-conserved order parameter (ϕ^i) to indicate the regions of the four precipitated phases. Composition $c_i(\mathbf{r}, t)$ is given as follows [9]:

$$
\begin{aligned}
c_i(\mathbf{r}, t) = c_i^{T3}(\mathbf{r}, t)h(\phi^{T3}) + c_i^{T6}(\mathbf{r}, t)h(\phi^{T6}) \\
+ c_i^{T7}(\mathbf{r}, t)h(\phi^{T7}) + c_i^{\alpha}(\mathbf{r}, t)[1 - \textstyle\sum_\theta h(\phi^\theta)]
\end{aligned} \tag{1}
$$

where[12],

$$h(\phi^\theta) = (\phi^\theta)^3[6(\phi^\theta)^2 - 15\phi^\theta + 10] \quad (2)$$

The local free energy density $G(c_i^\theta, t)$ of the system is expressed as follows:

$$G(c_i^\theta, t) = h(\phi^{T3})G^{T3} + h(\phi^{T6})G^{T6} + h(\phi^{T7})G^{T7} + [1 - \textstyle\sum_\theta h(\phi^\theta)]G^\alpha(c_i^\alpha, t) + g(\phi^\theta) \quad (3)$$

where,

$$G^\alpha(c_i^\alpha, t) = c_1^\alpha \times^0 G_{Fe}^{bcc} + c_2^\alpha \times^0 G_{Mn}^{bcc} + c_3^\alpha \times^0 G_{Ni}^{bcc} + c_4^\alpha \times^0 G_{Si}^{bcc} + RT[c_1^\alpha log(c_1^\alpha) + c_2^\alpha log(c_2^\alpha) + c_3^\alpha log(c_3^\alpha) + c_4^\alpha log(c_4^\alpha)] + L_{Fe,Mn}^{bcc} c_1^\alpha c_2^\alpha + L_{Fe,Ni}^{bcc} c_1^\alpha c_3^\alpha + L_{Fe,Si}^{bcc} c_1^\alpha c_4^\alpha + L_{Mn,Ni}^{bcc} c_2^\alpha c_3^\alpha + L_{Mn,Si}^{bcc} c_2^\alpha c_4^\alpha \quad (4)$$

where $c_1^\alpha = 1.0 - c_2^\alpha - c_3^\alpha - c_4^\alpha$.

From ref.[13], we obtain the free energy of each element of the α phase.

The free energy of the $T3$, $T6$, and $T7$ precipitates is given as follows:

$$G^{T3} =^0 G_{Mn,Ni,Si}^{T3} \quad (5)$$

$$G^{T6}(c_i^{T6}, t) = y_3^{II} \times^0 G_{Mn,Ni}^{T6} + y_4^{II} \times^0 G_{Mn,Si}^{T6} + 2/3RT[y_3^{II} log(y_3^{II}) + y_4^{II} log(y_4^{II})] + y_3^{II} y_4^{II} L_{Mn:Ni,Si}^{bcc} \quad (6)$$

y_3^{II} and y_4^{II} denote the site fraction of Ni and Si at the second sub-lattice of the $T6$ phase, respectively.

$$G^{T7} =^0 G_{Mn,Ni,Si}^{T7} \quad (7)$$

4. Results

We performed a single particle simulation to examine whether our phase-field framework can generate consistent results with the predictions based on the thermodynamics. We also performed a set of simulations with two particles to understand the interplay between precipitates.

4.1 Single particle stability

We conducted the phase-field modeling with single second-phase particle. ($T3$,$T6$,$T7$). The initial circular particle radius is $1.5nm$ and the initial condition of matrix is $c_2^\alpha = 0.008$, $c_3^\alpha = 0.008$, $c_4^\alpha = 0.00808$ and $T = 550K$. We plotted the particle radius as time evolves in Fig. 1.

We performed CALPHAD modeling using ThermoCalc Software with the implementation of UW1 database [3] with same initial compositions of matrix. The equilibrium phases were $BCC(A2)$ (98.940 mol%) and $T6$ (1.363 mol%). Also, $T6$ phase is quite dominantly observed in neutron-irradiated RPV steel [3, 4, 5]. Therefore, we concluded that our phase-field modeling generates consistent results with CALPHAD modeling and former experimental studies.

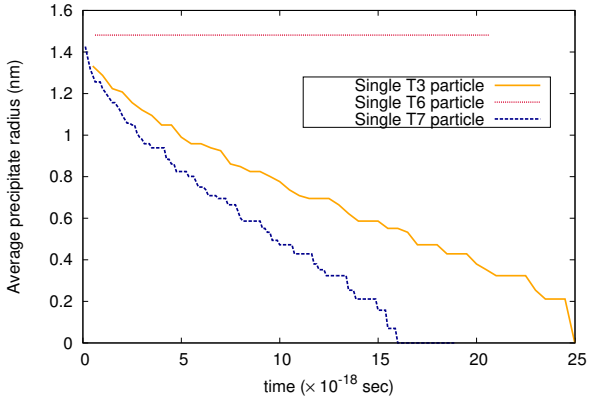

Fig. 1. Precipitate radius of $T3$, $T6$, and $T7$ precipitates with respect to time

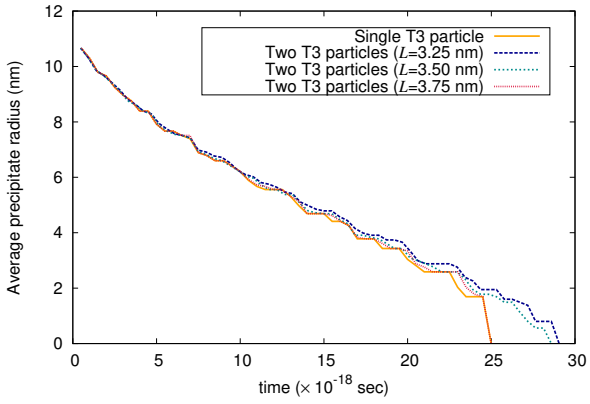

Fig. 2. Precipitate radius of single $T3$ and $T3-T3$ precipitates with different distance between particles (L).

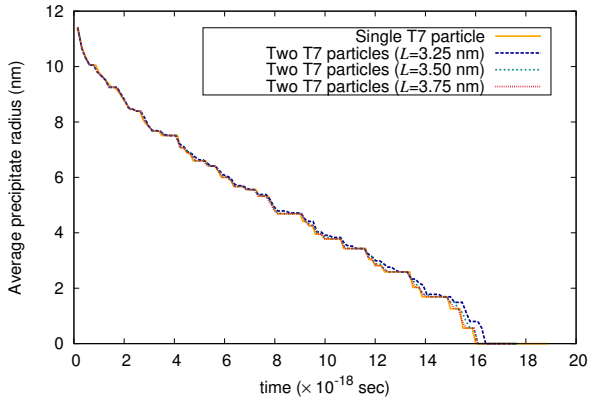

Fig. 3. Precipitate radius of single $T7$ and $T7-T7$ precipitates with different distance between particles (L).

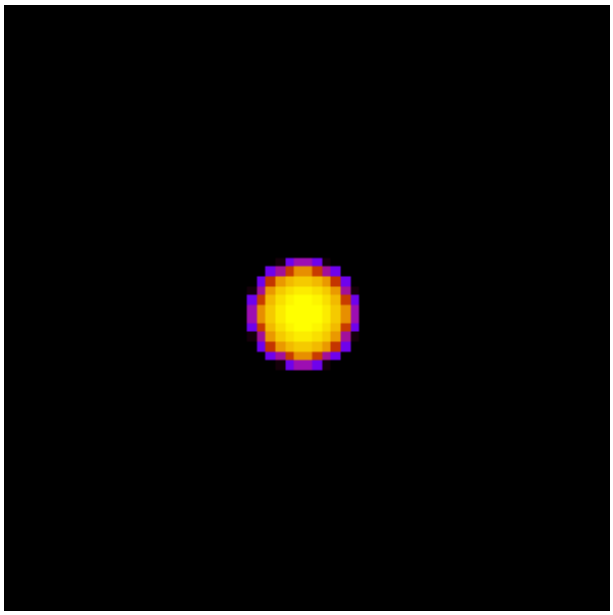

Fig. 4. ϕ^{T3} profile when $t = 1.5 \times 10^{-17}$ sec.

4.2 Particle stability under the interaction between particles

As we expected, we found that $T3$ particle remains longer when $T3$ particles interact comparing to a single $T3$ particle. Also, as the distance between particles $L = 3.75nm$, the shrinkage curve in Fig. 2 nearly converges to the curve of single T3 particle. Consistent results were observed for $T7$ precipitate in Fig. 3. we found that the particle morphology becomes droplet shaped in Fig. 2. The interfacial energy reducing is also a driving force for the morphological evolution in this study, the attraction force between particles are observed in Fig. 2. Since, the circle has the maximized mean curvature in 2D system, we expected that this morphological deviation can reduce the shrinkage rate.

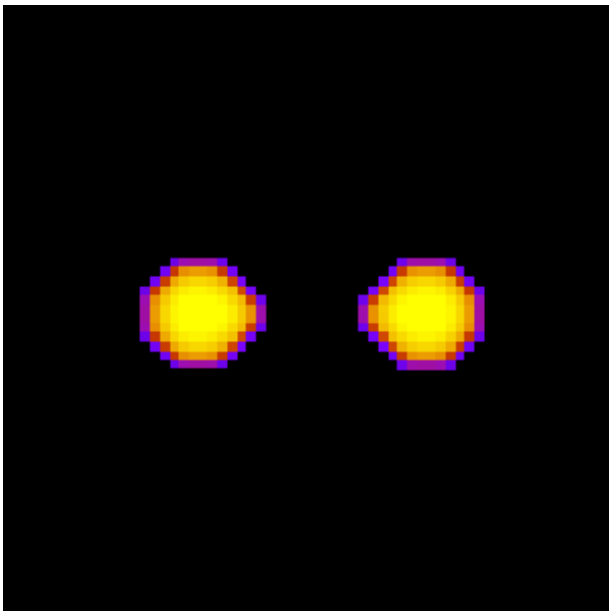

Fig. 5. ϕ_1^{T3} and ϕ_2^{T3} profiles when $t = 1.5 \times 10^{-17}$ sec. The distance between particle center, $L = 3.25$ *nm*.

5. Conclusions

We performed the phase-field simulation to examine stability of a single precipitate and two precipitates. We found that our phase-field framework produce the consistent results of thermodynamic modeling and experimental observations. Our simulations reveal that the particle interaction expands the life span of particle.

References

1. G. ODETTE and G. LUCAS, "Embrittlement of nuclear reactor pressure vessels," *JOm*, **53**, *7*, 18–22 (2001).
2. G. ODETTE and G. LUCAS, "Recent progress in understanding reactor pressure vessel steel embrittlement," *Radiation effects and defects in solids*, **144**, *1-4*, 189–231 (1998).
3. W. XIONG, H. KE, R. KRISHNAMURTHY, P. WELLS, L. BARNARD, G. R. ODETTE, and D. MORGAN, "Thermodynamic models of low-temperature Mn–Ni–Si precipitation in reactor pressure vessel steels," *MRS Communications*, **4**, *03*, 101–105 (2014).
4. D. SPROUSTER, J. SINSHEIMER, E. DOORYHEE, S. GHOSE, P. WELLS, T. STAN, N. ALMIRALL, G. ODETTE, and L. ECKER, "Structural characterization of nanoscale intermetallic precipitates in highly neutron irradiated reactor pressure vessel steels," *Scripta Materialia*, **113**, 18–22 (2016).
5. P. B. WELLS, T. YAMAMOTO, B. MILLER, T. MILOT, J. COLE, Y. WU, and G. R. ODETTE, "Evolution of manganese–nickel–silicon-dominated phases in highly irradiated reactor pressure vessel steels," *Acta Materialia*, **80**, 205–219 (2014).
6. T. KOYAMA and H. ONODERA, "Computer simulation of phase decomposition in Fe-Cu-Mn-Ni quaternary alloy

based on the phase-field method," *Materials transactions*, **46**, *6*, 1187–1192 (2005).
7. T. KOYAMA, K. HASHIMOTO, and H. ONODERA, "Phase-field simulation of phase transformation in Fe-Cu-Mn-Ni quaternary alloy," *Materials transactions*, **47**, *11*, 2765–2772 (2006).
8. S. BINER, W. RAO, and Y. ZHANG, "The stability of precepitates and the role of lattice defects in Fe-1at% Cu-1at% Ni-1at% Mn alloy: A phase-field model study," *Journal of Nuclear Materials*, **468**, 9–16 (2016).
9. S. G. KIM, W. T. KIM, and T. SUZUKI, "Phase-field model for binary alloys," *Physical review e*, **60**, *6*, 7186 (1999).
10. J. W. CAHN and J. E. HILLIARD, "Free energy of a nonuniform system. I. Interfacial free energy," *The Journal of chemical physics*, **28**, *2*, 258–267 (1958).
11. S. M. ALLEN and J. W. CAHN, "A microscopic theory for antiphase boundary motion and its application to antiphase domain coarsening," *Acta Metallurgica*, **27**, *6*, 1085–1095 (1979).
12. J. ZHU, T. WANG, A. ARDELL, S. ZHOU, Z. LIU, and L. CHEN, "Three-dimensional phase-field simulations of coarsening kinetics of γâĂš particles in binary Ni–Al alloys," *Acta Materialia*, **52**, *9*, 2837–2845 (2004).
13. A. DINSDALE, "SGTE data for pure elements," *Calphad*, **15**, *4*, 317–425 (1991).